Journal of Applied Polymer Science

Carbon nanohorn-graphene nanoplate hybrid: An excellent electrode material for supercapacitor application

Sandip Maiti, Amit Kumar Das, Sumanta Kumar Karan, Bhanu B. Khatua
Materials Science Centre, Indian Institute of Technology, Kharagpur 721302, India
Correspondence to: B. B. Khatua (E-mail: khatuabb@matsc.iitkgp.ernet.in)

ABSTRACT: This study describes the capacitor behavior of carbon nanohorn (CNH)/graphene nanoplate (GNP) hybrid (CNGN). The well-CNH-decorated GNP-plate electrode materials show high capacitance value (≈677 F/g) and can be extensively used in new generation for energy storage. In the hybrid (CNGN), two nanofillers jointly affect the capacitance behavior and increase the capacitance value of the CNGN hybrid. Homogeneous coating of CNH over the GNP plate plays an effective role to enhance the capacitance behavior of the composite. Field emission scanning electron microscopy and high-resolution transmission electron microscopy analysis of the composite confirmed the CNH coating on the GNP plate. © 2015 Wiley Periodicals, Inc. J. Appl. Polym. Sci. **2015**, *132*, 42118.

KEYWORDS: applications; morphology; nanoparticles; nanowires and nanocrystals; properties and characterization

Received 12 November 2014; accepted 15 February 2015
DOI: 10.1002/app.42118

INTRODUCTION

Supercapacitors have been most valuable materials for energy storage applications in recent time. They have been highly demanded in various motor vehicles and portable electronic devices where energy storage is the key requirement. Owing to their rapid charging–discharging rates, long cycle life (>100, 000 cycles), and high power density,[1–3] they have been chosen as most promising materials for alternative energy sources in modern time for all kinds of electric devices.[4,5] Generally, supercapacitors are of two types and have been categorized based on their charge-storage mechanism:[6,7] (i) electrical double-layer capacitors and (ii) pseudocapacitors. In case of pseudocapacitors, metal oxides (NiO, MnO_2, etc) or conducting polymers have been used as electrode materials. In addition, Faradic reactions occur at the electrode–electrolyte interface and charge is stored faradaically by charge transfer between electrolyte and electrode. This process goes through electrosorption, reduction−oxidation reactions, and intercalation processes. Among them, pseudocapacitors could be the source of higher specific capacitance but it is very costly. So, preparation of low-cost and high-performance supercapacitor materials has now been a great challenge.

At present, carbon-based conducting nanofillers have been greatly used for the preparation of supercapacitor materials due to its nanosize, high aspect ratio, high surface area, and very high electrical conductivity.[8] In this regard, different carbon-based nanofillers such as carbon nanotube (CNT), graphene, and carbon nanohorn (CNH) have been considered as most promising electrode materials for supercapacitor applications. These carbon-based conducting nanofillers have greatly affected the electron transfer rate during faradaic charge transfer reactions in the composites and increased the capacitance value.[9] Single-walled carbon nanohorns (SWCNHs) look like dahlia flower with spherical superstructure of aggregated nano-sized graphitic tubes.[10–12] It has high surface area, internal nanospace, excellent porosity, and high electrical conductivity which are the key factors of CNHs. On the other hand, graphene nanoplate (GNP) is a plate-like structure and has high surface area and high conductivity in nature.

Several research groups are working on supercapacitor using graphene, CNT, or CNH as conducting nanofillers. For instance, Deshmukh *et al.*[13] have synthesized Fe_3O_4–SWCNH nanocomposites and the obtained specific capacitance value was ≈377 F/g at current density of 0.5 A/g. Shi and coworkers[14] have studied the capacitance performance of the chemically converted graphene and polyaniline (PANI) nanofibers composite. They observed the electrochemical capacitance of ≈210 F/g at a discharge rate of 0.3 A/g. Baek and coworkers[15] have synthesized PANI-grafted reduced graphene oxide composite. They have achieved capacitance value of ≈250 F/g with high electrical conductivity (≈8.66 S/cm). Wang *et al.*[16] have prepared one-dimensional and layered parallel folding of cobalt oxalate nanostructures for using as energy electrode material for

This article was published online on 13 March 2014. An error was subsequently identified. This notice is included in the online and print versions to indicate that both have been corrected 01 April 2014.

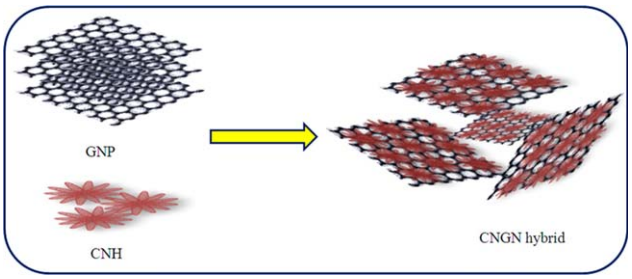

Figure 1. schematic diagram for the preparation of CNGN hybrid. [Color figure can be viewed in the online issue, which is available at wileyonlinelibrary.com.]

supercapacitor application. The reported capacitance value was ≈202.5 F/g at a current density of 1 A/g.

In this study, we have prepared CNGN hybrid through simple method. Thus, prepared CNGN hybrid shows very high specific capacitance value (∼677 F/g) at a scan rate of 5 mV/s. Owing to homogeneous coating of conducting CNH on GNP in the CNGN hybrid, it forms a conducting electron transfer path and provides more active sites for nucleation and increases the capacitance value of the hybrid.

EXPERIMENTAL

Materials Required

Potassium chloride was purchased from Merck, Germany. Single-layered CNH (carbon purity: >99%, horn diameter: 3∼5 nm, horn length: 30∼50 nm, cluster diameter: 60∼120 nm, density: 1.1 g/cm^3, surface area: 250∼300 m^2/g) was procured from J. K. Impex, Mumbai, India. Cetyl trimethylammonium bromide (CTAB) was purchased from Loba Chemie Pvt. Ltd India. Multi-layered GNP (carbon purity: >99.5%, thickness: 8∼10 nm, diameter: 5∼25 μm, electrical conductivity: 10^7 S/m) was purchased from J. K. Impex, Mumbai, India.

Preparation of the CNGN Hybrid

One hundred milliliters of de-ionized (DI) water was taken in a 500 ml beaker and 1 g of CTAB was added to it. The solution was stirred for few minutes to dissolve CTAB at room temperature. Then, 30 mg of CNH and 30 mg of GNP were added to it and the mixture was ultrasonicated for 1.5 h for homogeneous dispersion of CNH and GNP in the solution, followed by vigorous stirring for another 2 h with magnetic stirrer at room temperature. After that, the solution was filtered and washed with DI water several times. Thus, the obtained residue was air dried for 24 h for further characterizations. A schematic diagram for the preparation of CNGN hybrid was shown in Figure 1.

CHARACTERIZATIONS

Field Emission Scanning Electron Microscope (FESEM)

The morphology of the CNGN hybrid was studied using FESEM (FE-SEM, Carl Zeiss-SUPRA^{TM} 40), with an accelerating voltage of 5 kV. The sample was dispersed in ethanol and dropped on Al foil. Then, this prepared drop cast e sample was coated with a thin layer of gold (approx ∼ 5 nm) to avoid the electrical charging during scanning. This gold-coated sample was scanned in the vacuum order of 10^{-4} to 10^{-6} mm Hg.

High-Resolution Transmission Electron Microscope (HRTEM)

The TEM analysis of the CNGN hybrid was carried out by HRTEM (HRTEM, JEM-2100, JEOL, JAPAN), operated at an accelerating voltage of 200 kV. A small amount of the CNGN hybrid was dispersed in ethanol through sonication. Then, the dispersed suspension of CNGN hybrid was dropped on the copper (Cu) grid for HRTEM analysis.

Electrochemical Characterization

Electrochemical analysis of as-synthesized CNGN hybrid was performed by cyclic voltammetry (CV) with a 760D Potentiostat (CH Instruments, Inc.) electrochemical analyzer. A three-electrode system was employed for all measurements where CNGN-hybrid-coated glassy carbon electrode, Pt wire, and Ag/AgCl served as working, counter, and reference electrodes, respectively. Cyclic voltammogram was recorded at different scan rates from 5 to 100 mV/s within the potential window from −0.2 to 0.6 V in 1 (*M*) KCl.

Electrochemical impedance spectroscopic (EIS) measurement was carried out in the frequency range of 100 mHz–10 MHz. The specific capacitances (C_{sp}) of CNGN hybrid at different scan rates were calculated by using eq. (1):[17]

$$C_{sp} = \left(\int IdV\right)/vmV \quad (1)$$

Where, I is the response current density, V is the potential (V), v is the potential scan rate (mV/s), and m is the mass of the CNGN hybrid in the electrodes.

RESULTS AND DISCUSSION

Electrochemical Analysis

CV Analysis. We have studied the capacitive performances of the CNGN hybrid, as shown in Figure 2. The characterization was done at different scan rates (5, 10, 20, 30, 50, 80, and 100 mV/s) in a three-electrode configuration with applied potential. The specific capacitance value of any materials was calculated through the given relation:[17]

$$C_{sp} = \left(\int IdV\right)/vmV$$

Where, I represents the response current density, V is the potential (V), v signifies the potential scan rate (mV/s), and m stands for the mass of the used materials in the electrodes. The cyclic voltammogram curve for CNGN hybrid at different scan rates (5, 10, 20, 30, 50, 80, and 100 mV/s) was observed in Figure 2(a). The corresponding capacitance values of the composites at each scan rate were also calculated with the help of eq. (1). Thus, we have achieved the capacitance value (≈677 F/g) for the CNGN hybrid. So, this result indicated that in the presence of both nanofillers, capacitance value was greatly affected and highly increased. The probable reason behind this is that a strong π–π stacking interaction occurred among the conducting GNP and CNH nanofillers, which play a crucial role to enhance the capacitance value of the composite. Earlier, some works already reported using CNT and CNH.[18,19] In addition, GNPs are well and homogeneously coated by CNH in the CNGN hybrid (observed in Figure 6), which facilitate the easy ion transfer throughout the composite and reduce the ionic

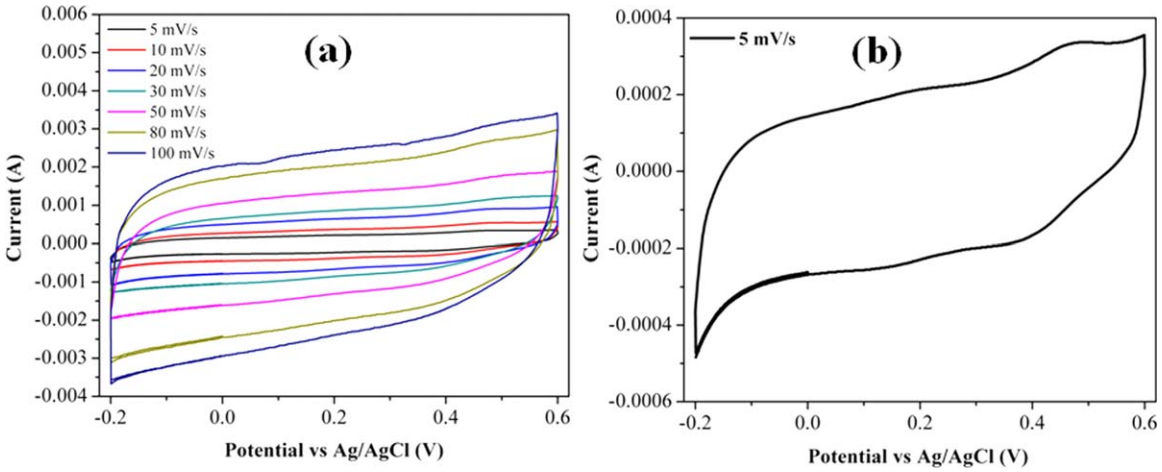

Figure 2. Cyclic voltammogram of CNGN hybrid (a) at different scan rates (5, 10, 20, 30, 50, 80 and 100 mV/s) and (b) at 5 mV/s. [Color figure can be viewed in the online issue, which is available at wileyonlinelibrary.com.]

diffusion path that act as a vital role to enhance the capacitance value of the composite. In addition, due to the presence of both conducting nanofillers (CNH and GNP) in the composite, a strong interconnecting conducting network structure is developed which is also responsible for high capacitance value of the composite. Figure 2(b) shows the cyclic voltammogram curve for CNGN hybrid at 5 mV/s.

The variations of scan rate with specific capacitance of the CNGN hybrid are plotted together and are shown in Figure 3.

From this figure, it is observed that the specific capacitance values gradually decreased with the increasing scan rate. With the increasing scan rate, diffusion resistance and electrochemical polarization effect become high which help to reduce the capacitance value of the materials.[20]

Cycle-Life Stability Test. For the comprehensive understanding of cyclic stability of the CNGN hybrid, we have calculated its specific capacitance after a particular cycle and then plotted the obtained capacitance values against the cycle numbers, as shown in Figure 4. The specific capacitance value of the composites gradually decreases with increasing cycle number.[21] The cycle stability of the CNGN hybrid was measured through repeating the CV in 1 *M* KCl electrolyte and studied at a scan rate of 10 mV/s for 1000 cycles. Thus, 81% of specific capacitance value retained after 1000 cycles. The π–π stacking interaction between the conducting GNP and CNH nanofillers resist the changing of regular network structure in the composites and improved the cyclic stability of composites.

EIS Analysis. Figure 5 shows the Nyquist plot of impedance and their fitting circuit for the CNGN hybrid which is carried out in the frequency region from 100 mHz to 10 MHz. Real component (Z′) and imaginary component (Z″) are the two components shown in Nyquist plot of impedance. The real component (Z′) of the composites stands for the ohmic properties, whereas the imaginary component (Z″) for the capacitive properties.[22] In general, ideal supercapacitor has three

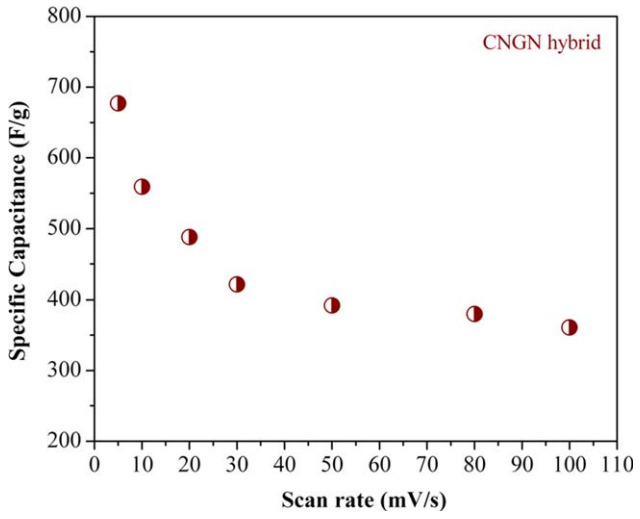

Figure 3. Plot of specific capacitance vs. scan rate for CNGN hybrid. [Color figure can be viewed in the online issue, which is available at wileyonlinelibrary.com.]

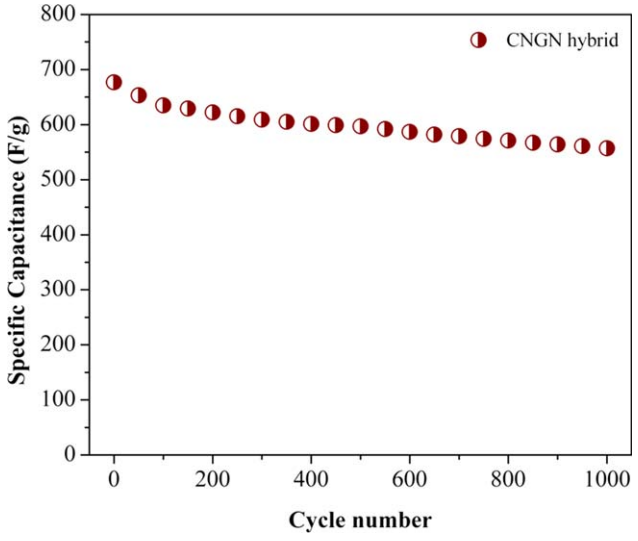

Figure 4. Specific capacitance vs. cycle number of CNGN hybrid in 1 (*M*) KCl solution. [Color figure can be viewed in the online issue, which is available at wileyonlinelibrary.com.]

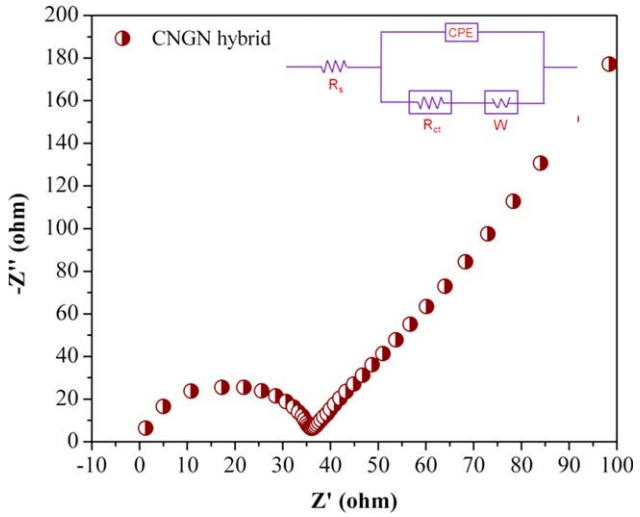

Figure 5. Nyquist plot and equivalent electrical circuit used in EIS fitting data of CNGN hybrid. [Color figure can be viewed in the online issue, which is available at wileyonlinelibrary.com.]

frequency-dependent regions in the Nyquist plot.[23] At the high-frequency region, the supercapacitor material is a pure resistor. The electrode porosities are seen at medium-frequency region where the electrolyte penetrates deeper and deeper into the porous structure of the electrode for decreasing the frequency from the very high-frequency region and results in a huge numbers of electrode surface for ion adsorption. This region is known as Warburg curve in the Nyquist plot of impedance. The capacitive behavior of the material was observed at low-frequency region of the plot where the imaginary part sharply increases and a vertical line is obtained. Ideal supercapacitor in real world does not exist. Solution resistance (R_s) of the composites is obtained from the intercepts in highest frequency of the curves at real axis.

The charge transfer resistance (R_{ct}) is estimated from the depressed semicircle curve which is shown at the higher frequency region of the Nyquist plot. Warburg resistance (W) of the composites is seen at intermediate frequency region. The constant phase element means the nonideal behavior of the supercapacitor and is expressed by n.[24] The Nyquist plots were analyzed by fitting the experimental impedance spectra to an equivalent electrical circuit, shown in the inset of Figure 5 which is schematically drawn. The π–π stacking interaction between the GNP and CNH plays a crucial role to help for efficient electrolyte accessibility to the electrode surface through shortening the ion diffusion path. The obtained vertical line at low-frequency region indicates the good capacitive behavior and low diffusion resistance of the electrode material. The supercapacitor will behave as an ideal when n value will be equal to one. It will behave as an insulator, when n is zero. In our study, n value is 0.76 ($>$0.5), which indicates the moderate capacitive behavior of CNGN hybrid.

Morphological Study

The morphology of the CNGN hybrid was well studied and shown in Figure 6. The FESEM images of the composite were seen in Figure 6(a,b). From these images, it is clearly observed that GNPs are homogeneously coated with CNH. This homogeneous coating of CNH over the GNP plays an important role to enhance the capacitance value of the composite. This homogeneous coating developed a strong π–π stacking interaction among the conducting nanofillers, which facilitates the easy electron transfer throughout the composite and increases the

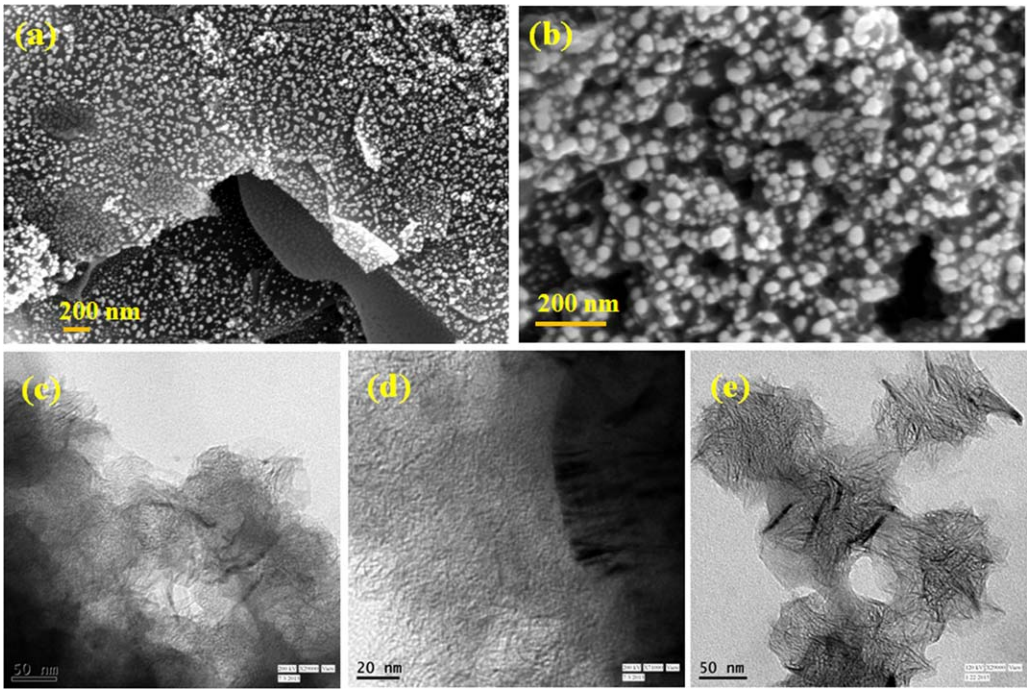

Figure 6. (a, b) FESEM micrographs of CNGN hybrid at two different magnifications. HRTEM micrographs of (c, d) CNGN hybrid at different magnifications and (e) pure CNH. [Color figure can be viewed in the online issue, which is available at wileyonlinelibrary.com.]

specific capacitance value of the composite. The HRTEM study of the CNGN hybrid also analyzed the morphology of the composite. The HRTEM images of the CNGN hybrid were shown in Figure 6(c,d) at different magnifications. These images also supported the homogeneous coating of CNH over the GNP platelets. So, homogeneous coating of CNH on GNP has played a crucial role in obtaining the high capacitance value of the composite compared to pure nanofillers. Figure 6(e) is the HRTEM image of pure CNH.

Comparative Study

Several researchers have already reported the specific capacitance values for different composites-based different nanofillers. Wang *et al.*[25] have used *in-situ* polymerization-reduction/dedoping–redoping process for the preparation of PANI/flexible graphene hybrid. They got high specific capacitance value of ≈1126 F/g. Huang and coworkers[26] have studied the capacitance value of PANI/graphene composites and achieved capacitance value of ≈640 F/g. The composite was prepared by *in-situ* polymerization of aniline in the presence of graphite oxide. Li *et al.*[27] have studied the specific capacitance value of the PANI nanofiber/graphene nanosheets composites. They reported comparatively high specific capacitance value of ≈ 1130 F/g at 5 mV/s scan rate for the composite. Zhang *et al.*[28] have prepared PANI-doped graphene composite by simple method. They have studied the capacitance value of the composite and the obtained value is ≈480 F/g at a current density of 0.1 A/g. Liu *et al.*[29] have prepared capacitor material through *in-situ* polymerization of aniline in the presence of flexible graphene sheet and the reported value is ≈301 F/g. Wang *et al.*[30] have chose PANI and flexible graphene for the preparation of PANI/flexible graphene composites to study the capacitance performance of the material. The reported gravimetric capacitance and volumetric capacitance of the composite were ≈233 F/g and ≈135 F/cm^3, respectively. Sahoo *et al.*[31] have prepared polypyrrole (PPy)/graphene composites through *in-situ* polymerization and reported capacitance value was ≈466 F/g at 10 mV/s scan rate. Fray and coworkers[32] have prepared highly porous nanorod-PANI/graphene composites and checked the capacitance performance of the porous material. They have achieved the capacitance value of ≈878.57 F/g at a current density of 1 A/g. Yu and coworkers[33] have prepared PANI nanorods/flexible graphene composites. Thus, obtained PANI nanorods/flexible graphene composites show specific capacitance value of ≈763 F/g. Lee and coworkers[34] have reported capacitance value of ≈637 F/g at 2 mV/s scan rate for MnO_2/SnO_2 composite. Feng *et al.*[35] prepared MnO_2/graphene composites by hydrothermal method. The obtained specific capacitance value was ≈516.8 F/g at a scan rate of 1 mV/s. Fan *et al.*[36] have prepared PANI-hollow spheres by electrochemically reduced graphene oxide. The specific capacitance of hybrid was ≈614 F/g at a current density of 1 A/g. Chang *et al.*[37] have prepared PANI/MWCNT nanocomposites. The obtained specific capacitance was ≈535 F/g at a current density of 1 A/g for 5 wt % MWCNT loading. Qian *et al.*[38] have prepared CNT/PPy core/shell composites. The reported specific capacitance was ≈276.3 F/g at current density of 1 A/g. In the present study, comparatively high capacitance value (≈677 F/g) was achieved at 5 mV/s scan rate for CNGN hybrid compared to most of the above reported methods.

CONCLUSION

This article discusses the capacitance performances of the CNGN hybrid. The hybrid was prepared by a simple method in the presence of two different conducting nanofillers, GNP and CNH. The homogeneous dispersion of the nanofillers (GNP and CNH) in the solution was carried out in the presence of CTAB through strong ultrasonication. The uniform coating of CNH over the GNP helped to increase the specific capacitance value of the CNGN hybrid. The presence of two conducting nanofillers in the hybrid makes a strong π–π stacking interaction among them and this interaction plays a crucial role in enhancing the capacitance value (≈677 F/g) of the hybrid. Thus, the prepared CNGN hybrid is considered as most promising electrode material for supercapacitor applications. In addition, the capacitive behavior and the morphology of the CNGN hybrid were thoroughly characterized.

ACKNOWLEDGMENTS

The authors acknowledge CSIR, New Delhi, India for their financial support.

REFERENCES

1. Tang, P.; Han, L.; Zhang, L. *ACS Appl. Mater. Inter.* **2014**, *6*, 10506.
2. Miller, J. R.; Simon, P. *Science* **2008**, *321*, 651.
3. Jang, B. Z.; Liu, C.; Neff, D.; Yu, Z.; Wang, M. C.; Xiong, W.; Zhamu, A. *Nano Lett.* **2011**, *11*, 3785.
4. Mao, B. S.; Wen, Z.; Bo, Z.; Chang, J.; Huang, X.; Chen, J. *ACS Appl. Mater. Inter.* **2014**, *6*, 9881.
5. Khilari, S.; Pandit, S.; Ghangrekar, M. M.; Pradhan, D.; Das, D. *Ind. Eng. Chem. Res.* **2013**, *52*, 11597.
6. Simon, P.; Gogotsi, Y. *Nature Mater.* **2008**, *7*, 845.
7. Khilari, S.; Pandit, S.; Das, D.; Pradhan, D. *Biosens. Bioelectron.* **2014**, *54*, 534.
8. Maiti, S.; Shrivastava, N. K.; Suin, S.; Khatua, B. B. *ACS Appl. Mater. Inter.* **2013**, *5*, 4712.
9. Lee, J. W.; Hall, A. S.; Kim, J.-D.; Mallouk, T. E. *Chem. Mater.* **2012**, *24*, 1158.
10. Zhu, S.; Xu, G. *Nanoscale* **2010**, *2*, 2538.
11. Chatterjee, S.; Carter, R.; Oakes, L.; Erwin, W. R.; Bardhan, Rizia.; Pint, C. L. *J. Phys. Chem. C* **2014**, *118*, 10893.
12. Maiti, S.; Khatua, B. B. *RSC Adv.* **2013**, *3*, 12874.
13. Deshmukh, A. B.; Shelke, M. V. *RSC Adv.* **2013**, *3*, 21390.
14. Wu, Q.; Xu, Y.; Yao, Z.; Liu, A.; Shi, G. *ACS Nano* **2010**, *4*, 1963.
15. Kumar, N. A.; Choi, H.-J.; Shin, Y. R.; Chang, D. W.; Dai, L.; Baek, J.-B. *ACS Nano* **2012**, *6*, 1715.
16. Wang, D.; Wang, Q.; Wang, T. *Inorg. Chem.* **2011**, *50*, 6482.
17. Yan, J.; Wei, T.; Shao, B.; Fan, Z.; Qian, W.; Zhang, M.; Wei, F. *Carbon* **2010**, *48*, 487.

18. Izadi-Najafabadi, Ali.; Yamada, T.; Futaba, D. N.; Yudasaka, M.; Takagi, H.; Hatori, H.; Iijima, S.; Hata, K. *ACS Nano* **2011**, *5*, 811.
19. Hiralal, P.; Wang, H.; Unalan, H. E.; Liu, Y.; Rouvala, M.; Wei, Di.; Andrew, P.; Amaratunga, G. A. J. *J. Mater. Chem.* **2011**, *21*, 17810.
20. Zhang, Y.; Li, G.-Y.; Lv, Y.; Wang, L.-Z.; Zhang, A.-Q.; Song, Y.-H.; Huang, B.-L. *Int. J. Hydrogen Energy* **2011**, *36*, 11760.
21. Ghosh, D.; Giri, S.; Moniruzzaman, M.; Basu, T.; Mandol, M.; Das, C. K. *Dalton Trans.* **2014**, *43*, 11067.
22. Chen, W.; Rakhi, R. B.; Hu, L.; Xie, X.; Cui, Y.; Alshareef, H. N. *Nano Lett.* **2011**, *11*, 5165.
23. Cheng, Q.; Tang, J.; Ma, J.; Zhang, H.; Shinya, N.; Qin, L.-C. *J. Phys. Chem. C* **2011**, *115*, 23584.
24. Yuge, R.; Miyawaki, J.; Ichihashi, T.; Kuroshima, S.; Yoshitake, T.; Ohkawa, T.; Aoki, Y.; Iijima, S.; Yudasaka, M. *ACS Nano* **2010**, *4*, 7337.
25. Wang, H.; Hao, Q.; Yang, X.; Lu, L.; Wang, X. *Nanoscale* **2010**, *2*, 2164.
26. Feng, X.-M.; Li, R.-M.; Ma, Y.-W.; Chen, R.-F.; Shi, N.-E.; Fan, Q.-L.; Huang, W. *Adv. Func. Mater.* **2011**, *21*, 2989.
27. Li, J.; Xie, H.; Li, Y.; Liu, J.; Li, Z. *J. Power Sources* **2011**, *196*, 10775.
28. Zhang, D.; Zhang, X.; Chen, Y.; Yu, P.; Wang, C.; Ma, Y. *J. Power Sources* **2011**, *196*, 5990.
29. Liu, S.; Liu, X.; Li, Z.; Yang, S.; Wang, J. *New J. Chem.* **2011**, *35*, 369.
30. Wang, D.-W.; Li, F.; Zhao, J.; Ren, W.; Chen, Z.-G.; Tan, J.; Wu, Z.-S.; Gentle, I.; Lu, G. Q.; Cheng, H.-M. *ACS Nano* **2009**, *3*, 1745.
31. Sahoo, S.; Dhibar, S.; Hatui, G.; Bhattacharya, P.; Das, C. K. *Polymer* **2013**, *54*, 1033.
32. Hu, L.; Tu, J.; Jiao, S.; Hou, J.; Zhua, H.; Fray, D. J. *Phys. Chem. Chem. Phys.* **2012**, *14*, 15652.
33. Cong, H.-P.; Ren, X.-C.; Wang, P.; Yu, S.-H. *Energy Environ. Sci.* **2013**, *6*, 1185.
34. Yan, J.; Khoo, E.; Sumboja, A.; Lee, P. S. *ACS Nano* **2010**, *4*, 4247.
35. Feng, X.; Yan, Z.; Chen, N.; Zhang, Y.; Ma, Y.; Liu, X.; Fan, Q.; Wang, L.; Huang, W. *J. Mater. Chem. A* **2013**, *1*, 12818.
36. Fan, W.; Zhang, C.; Tjiu, W. W.; Pramoda, K. P.; He, C.; Liu, T. *ACS Appl. Mater. Inter.* **2013**, *5*, 3382.
37. Chang, C.-M.; Weng, C.-J.; Chien, C.-M.; Chuang, T.-L.; Lee, T.-Y.; Yeh, J.-M.; Wei, Y. *J. Mater. Chem. A* **2013**, *1*, 14719.
38. Qian, T.; Zhou, X.; Yu, C.; Wu, S.; Shen, J. *J. Mater. Chem. A* **2013**, *1*, 15230.